J|A|C|S ARTICLES

Published on Web 01/08/2009

Impact of Perfluorination on the Charge-Transport Parameters of Oligoacene Crystals

M. Carmen Ruiz Delgado,[†] Kathryn R. Pigg,[†] Demétrio A. da Silva Filho,[†] Nadine E. Gruhn,[‡,⊥] Youichi Sakamoto,[§] Toshiyasu Suzuki,[§] Reyes Malavé Osuna,[||] Juan Casado,[||] Víctor Hernández,[||] Juan Teodomiro López Navarrete,[||] Nicolas G. Martinelli,[#] Jérôme Cornil,[#] Roel S. Sánchez-Carrera,[†] Veaceslav Coropceanu,[†] and Jean-Luc Brédas*[,†]

School of Chemistry and Biochemistry and Center for Organic Photonics and Electronics, Georgia Institute of Technology, Atlanta, Georgia 30332-0400, Department of Chemistry, University of Arizona, Tucson, Arizona 85721-0041, Institute for Molecular Science, Myodaiji, Okazaki 444-8787, Japan, Department of Physical Chemistry, University of Málaga, 29071-Málaga, Spain, and Laboratory for Chemistry of Novel Materials, Center for Research in Molecular Electronics and Photonics, University of Mons-Hainaut, Place du Parc 20, B-7000 Mons, Belgium

Received September 22, 2008; E-mail: jean-luc.bredas@chemistry.gatech.edu

Abstract: The charge-transport parameters of the perfluoropentacene and perfluorotetracene crystals are studied with a joint experimental and theoretical approach that combines gas-phase ultraviolet photoelectron spectroscopy and density functional theory. To gain a better understanding of the role of perfluorination, the results for perfluoropentacene and perfluorotetracene are compared to those for their parent oligoacenes, that is, pentacene and tetracene. Perfluorination is calculated to increase the ionization potentials and electron affinities by ~1 eV, which is expected to reduce significantly the injection barrier for electrons in organic electronics devices. Perfluorination also leads to significant changes in the crystalline packing, which greatly affects the electronic properties of the crystals and their charge-transport characteristics. The calculations predict large conduction and valence bandwidths and low hole and electron effective masses in the perfluoroacene crystals, with the largest mobilities expected along the π-stacks. Perfluorination impacts as well both local and nonlocal vibrational couplings, whose strengths increase by a factor of about 2 with respect to the parent compounds.

1. Introduction

Oligoacenes such as tetracene and pentacene, see Figure 1, are among the most promising classes of organic semiconductors for (opto)electronic applications.[1,2] The planarity of the oligoacene molecules, which facilitates tight crystal packing, and the extension of the π-system over the whole molecules enable large intermolecular wave function overlaps. Organic thin-film transistors (OTFTs) based on tetracene deposited on SiO_2 display hole field-effect mobilities as high as 0.15 $cm^2/(V \cdot s)$ at room temperature.[3] Even higher mobilities, up to 2.4 $cm^2/(V \cdot s)$, are observed for devices fabricated directly from single crystals;[4] it is useful to note that such mobility values exceed those of amorphous silicon. Among tetracene derivatives, the single crystals of 5,6,11,12-tetraphenyltetracene (commonly known as rubrene) present remarkable hole mobilities on the order of 20 $cm^2/(V \cdot s)$ at room temperature.[5] Pentacene also shows some of the highest hole mobilities reported so far for OTFTs with values as high as 5.5 $cm^2/(V \cdot s)$.[6] Despite the successes with hole transport in oligoacenes, it has turned out to be more difficult to achieve n-type transport in these materials. For instance, pentacene OTFTs exhibit electron mobilities of ca. 0.04 $cm^2/(V \cdot s)$.[7] To produce bipolar transistors and complementary circuits, it would be ideal to have both n-type and p-type organic semiconductors with similar physical and electrical properties.[8−10]

[†] Georgia Institute of Technology.
[‡] University of Arizona.
[§] Institute for Molecular Science.
[||] University of Málaga.
[#] University of Mons-Hainaut.
[⊥] Current address: Department of Chemistry, University of Washington, Seattle, WA 98185-1700.

(1) Anthony, J. E. *Chem. Rev.* **2006**, *106*, 5028.
(2) Anthony, J. E. *Angew. Chem., Int. Ed.* **2008**, *47*, 452.
(3) Cicoira, F.; Santato, C.; Dinelli, F.; Murgia, M.; Loi, M. A.; Biscarini, T.; Zamboni, R.; Heremans, P.; Muccini, M. *Adv. Funct. Mater.* **2005**, *15*, 375.
(4) Reese, C.; Chung, W. J.; Ling, M. M.; Roberts, M.; Bao, Z. N. *Appl. Phys. Lett.* **2006**, *89*, 202108.
(5) Podzorov, V.; Menard, E.; Borissov, A.; Kiryukhin, V.; Rogers, J. A.; Gershenson, M. E. *Phys. Rev. Lett.* **2004**, *93*, 086602.
(6) Lee, S.; Koo, B.; Shin, J.; Lee, E.; Park, H.; Kim, H. *Appl. Phys. Lett.* **2006**, *88*, 162109.
(7) Singh, T. B.; Senkarabacak, P.; Sariciftci, N. S.; Tanda, A.; Lackner, C.; Hagelauer, R.; Horowitz, G. *Appl. Phys. Lett.* **2006**, *89*, 033512.
(8) Dodabalapur, A.; Katz, H. E.; Torsi, L.; Haddon, R. C. *Science* **1995**, *269*, 1560.
(9) Dodabalapur, A.; Katz, H. E.; Torsi, L.; Haddon, R. C. *Appl. Phys. Lett.* **1996**, *68*, 1108.
(10) Lin, Y. Y.; Dodabalapur, A.; Sarpeshkar, R.; Bao, Z.; Li, W.; Baldwin, K.; Raju, V. R.; Katz, H. E. *Appl. Phys. Lett.* **1999**, *74*, 2714.

 10.1021/ja807528w CCC: $40.75

A successful strategy developed to convert a p-type organic semiconductor into n-type without greatly affecting the molecular structure is to functionalize the π-conjugated core with fluorine atoms.[11−16] Fluorine is the most electronegative element and is relatively small in size (hydrogen < fluorine < carbon). Fluorination increases the electron affinity (in absolute terms) with respect to the parent molecule and, as a result, generally improves electron injection. Some of us have recently reported the synthesis of perfluorotetracene and perfluoropentacene and demonstrated that perfluorination is a viable route to create n-channel semiconductors from acenes.[17−19] Transistors based on perfluoropentacene exhibit electron mobilities as high as 0.22 $cm^2/(V \cdot s)$, and the combination of perfluoropentacene (n-channel) and pentacene (p-channel) offers the possibility to fabricate bipolar transistors and complementary circuits.[17−19]

To gain a better understanding of the effects of perfluorination, our goal here is to compare the electronic properties of perfluoropentacene (**PFP**) and perfluorotetracene (**PFT**) with those of their parent molecules, that is, pentacene (**PEN**) and tetracene (**TET**); see Figure 1. We have used a joint experimental and theoretical approach involving high-resolution gas-phase ultraviolet photoelectron spectroscopy (UPS) and density functional theory (DFT). To rationalize the inversion of transport channel upon perfluorination (i.e., from p-type to n-type) and to establish structure−property relationships, we investigate not only the structural and electronic properties at the molecular level but also the properties of the corresponding crystal structures.

2. Methodology

2.1. Experimental and Theoretical Details. 2.1.1. Experimental Techniques. The **PFT** and **PFP** compounds were synthesized as previously described in refs 17−19. Gas-phase UPS spectra (He I) were recorded at the University of Arizona on an instrument built around a 36 cm radius, 8 cm gap hemispherical analyzer (McPherson, 10 cm gap) using a custom-designed photon source and collection methods. Instrument control and electron counting are provided by a National Instruments PCIe-6259 multifunction DAQ board and custom software. Samples sublimed cleanly with no evidence for decomposition in the gas phase or as a solid residue. Sublimation temperatures, as monitored with a K-type thermocouple passed through a vacuum feed and attached directly to the ionization cell (10^{-4} Torr), were 200−270 °C for **PFT** and 230−290 °C for **PFP**. The argon $^2P_{3/2}$ ionization at 15.759 eV was used as an internal calibration lock of the absolute ionization energy, and its difference with the CH_3I $^2E_{1/2}$ ionization at 9.538 eV provided an external calibration of the energy scale. The instrument resolution (measured as the full width at half-maximum (fwhm) of the argon $^2P_{3/2}$ ionization) was 0.026−0.030 eV during data collection. The intensity of the spectra was corrected according to an experimentally determined analyzer sensitivity function. The He I spectra were also corrected for He I β resonance line emission from the source, which is about 3% of the intensity of the He I α line emission and at 1.869 eV higher photon energy.

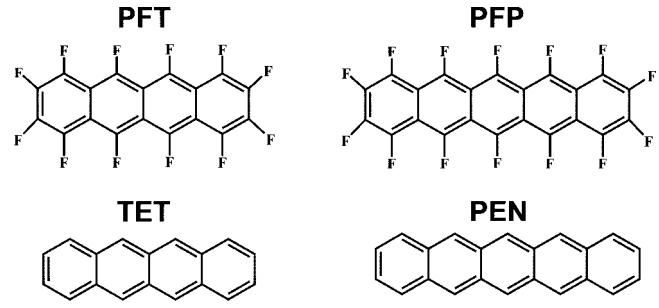

Figure 1. Chemical structures of the oligoacenes examined in this study with the notation used throughout the text: **PFT** = perfluorotetracene; **PFP** = perfluoropentacene; **TET** = tetracene; and **PEN** = pentacene.

2.1.2. Computational Methods. The molecular geometries of the neutral and radical-ion states were calculated at the Density Functional Theory (DFT) level using the B3LYP functional[20,21] and the 6-31G** basis[22−24] set, as implemented in the Gaussian 03 program.[25] The vibrational frequencies and related normal coordinates were calculated at the same computational level. Single-point calculations were also performed using the valence-double-ζ basis set augmented with s and p diffuse functions for both C and F atoms and s diffuse functions for hydrogen.[26]

The intramolecular reorganization energy (λ) associated with an intermolecular electron-transfer reaction consists of two terms related to the geometry relaxation energies upon going from the neutral state to a charged molecular state and vice versa; it is given by:[27]

$$\lambda = \lambda_{rel}^{(1)} + \lambda_{rel}^{(2)} \quad (1)$$

The terms $\lambda_{rel}^{(1)}$ and $\lambda_{rel}^{(2)}$ were computed directly from the adiabatic potential-energy surfaces (see Figure 2) as:

$$\lambda_{rel}^{(1)} = E^{(1)}(M) - E^{(0)}(M) \quad (2)$$

$$\lambda_{rel}^{(2)} = E^{(1)}(M^{\bullet}) - E^{(0)}(M^{\bullet}) \quad (3)$$

Here, $E^{(0)}(M)$ and $E^{(0)}(M^{\bullet})$ are the ground-state energy of the neutral state and the energy of the charged (cation or anion) molecular state, respectively; $E^{(1)}(M)$ is the energy of the neutral molecule at the optimal ion geometry, and $E^{(1)}(M^{\bullet})$ is the energy of the ionized state at the optimal geometry of the neutral molecule. The contribution of each vibrational mode to λ_{rel} was obtained by expanding the total energies of the neutral and charged molecules in a power series of normal coordinates. In the harmonic approximation, the relaxation energy λ_{rel} is:

$$\lambda_{rel} = \sum \lambda_i = \sum \hbar\omega S_i \quad (4)$$

(11) Facchetti, A.; Yoon, M. H.; Stern, C. L.; Katz, H. E.; Marks, T. J. *Angew. Chem., Int. Ed.* **2003**, *42*, 3900.
(12) Bao, Z. A.; Lovinger, A. J.; Brown, J. *J. Am. Chem. Soc.* **1998**, *120*, 207.
(13) Facchetti, A.; Mushrush, M.; Katz, H. E.; Marks, T. J. *Adv. Mater.* **2003**, *15*, 33.
(14) Heidenhain, S. B.; Sakamoto, Y.; Suzuki, T.; Miura, A.; Fujikawa, H.; Mori, T.; Tokito, S.; Taga, Y. *J. Am. Chem. Soc.* **2000**, *122*, 10240.
(15) Sakamoto, Y.; Suzuki, T.; Miura, A.; Fujikawa, H.; Tokito, S.; Taga, Y. *J. Am. Chem. Soc.* **2000**, *122*, 1832.
(16) Yoon, M. H.; Facchetti, A.; Stern, C. E.; Marks, T. J. *J. Am. Chem. Soc.* **2006**, *128*, 5792.
(17) Sakamoto, Y.; Suzuki, T.; Kobayashi, M.; Gao, Y.; Fukai, Y.; Inoue, Y.; Sato, F.; Tokito, S. *J. Am. Chem. Soc.* **2004**, *126*, 8138.
(18) Inoue, Y.; Sakamoto, Y.; Suzuki, T.; Kobayashi, M.; Gao, Y.; Tokito, S. *Jpn. J. Appl. Phys., Part 1* **2005**, *44*, 3663.
(19) Sakamoto, Y.; Suzuki, T.; Kobayashi, M.; Gao, Y.; Inoue, Y.; Tokito, S. *Mol. Cryst. Liq. Cryst.* **2006**, *444*, 225.
(20) Becke, A. D. *J. Chem. Phys.* **1993**, *98*, 5648.
(21) Lee, C. T.; Yang, W. T.; Parr, R. G. *Phys. Rev. B* **1988**, *37*, 785.
(22) Harihara, P. C.; Pople, J. A. *Theor. Chim. Acta* **1973**, *28*, 213.
(23) Hehre, W. J.; Ditchfield, R.; Pople, J. A. *J. Chem. Phys.* **1972**, *56*, 2257.
(24) Francl, M. M.; Pietro, W. J.; Hehre, W. J.; Binkley, J. S.; Gordon, M. S.; Defrees, D. J.; Pople, J. A. *J. Chem. Phys.* **1982**, *77*, 3654.
(25) Frisch, M. J. *Gaussian 03*, revision B.02; Gaussian, Inc.: Pittsburgh, PA, 2003.
(26) Clark, T.; Chandrasekhar, J.; Spitznagel, G. W.; Schleyer, P. V. *J. Comput. Chem.* **1983**, *4*, 294.
(27) Brédas, J. L.; Beljonne, D.; Coropceanu, V.; Cornil, J. *Chem. Rev.* **2004**, *104*, 4971.

$$\lambda_i = \frac{k_i}{2}\Delta Q_i^2 \quad S_i = {}^{\lambda_i}/_{\hbar\omega_i} \tag{5}$$

In these equations, the summations run over all vibrational modes; ΔQ_i represents the displacement along normal mode Q_i between the equilibrium geometries of the neutral and charged molecules; k_i and ω_i represent the corresponding force constants and vibrational frequencies; and S_i denotes the Huang−Rhys factor (hole- or electron-vibration coupling constant).

The ionization potentials (IPs) and electron affinities (EAs) were also calculated directly from the relevant points on the potential energy surfaces. Specifically, vertical IPs [EAs] were evaluated as the difference between the energy of the cation [anion] at the neutral geometry and that of the neutral species at the neutral geometry and adiabatic IPs [EAs] as the energy difference between the relaxed cation [anion] and the neutral molecule.

The Huang−Rhys factors were obtained by means of the DUSHIN code[28] and used to simulate the vibrational structure of the first ionization peak in the framework of the Born−Oppenheimer and Franck−Condon approximations according to the procedure described in detail elsewhere.[29] The frequencies were scaled down by the usual factor of 0.9613, which has been shown to reproduce the experimental frequencies very well.[30]

Transfer integrals for pairs of molecules taken out of the crystal structures were calculated at the DFT level by using a fragment orbital approach[31] in combination with a basis set orthogonalization procedure.[32] These calculations were performed with the PW91 functional and Slater-type triple-ζ plus polarization (TZP) basis sets, using the ADF (Amsterdam Density Functional) package.[33]

The thermal fluctuations of the electronic transfer integrals (see the vibronic coupling section below) were derived by combining molecular dynamics (MD) simulations and quantum-chemical calculations. The MD simulations were carried out in the Discover module of the Materials Studio package using the COMPASS force field,[34] which was validated for each crystal structure (**PFT**, **PFP**, and **PEN**) using the procedure developed by Cornil and coworkers.[35] First, the size of the supercell is chosen in such a way that molecular pairs (dimers) of interest are surrounded by a full shell of neighboring molecules to prevent artificial symmetry effects: (a) For **PFT**, a supercell with 288 molecules is initially created via a $3 \times 6 \times 4$ replica of the unit cell; (b) for **PFP**, a $4 \times 6 \times 3$ supercell with 144 molecules; and (c) for **PEN**, a $6 \times 3 \times 4$ supercell with 144 molecules. Each system was equilibrated for 150 ps (180 ps for **PFP**) using an Andersen thermostat in the NVT ensemble at 298 K and a time step of 1 fs. After equilibration, a simulation of 150 ps was run, and frames were extracted every 30 fs along the trajectory to give 5000 total frames. Because it is necessary to evaluate a very large number of transfer integrals, their calculations were performed at the semiempirical Hartree−Fock INDO level; note that the results from the INDO method are in very good agreement with those previously obtained at the DFT level.

The electronic band-structure calculations of **PFT** and **PFP** were performed with VASP[36−38] using the PBE[39] (Perdew−Burke−Ernzerhof) exchange-correlation functional and a plane-wave basis set. Electron−ion interactions were described using the projector augmented wave (PAW) method.[40,41] The kinetic energy cutoff on the wave function expansion was set to 400 eV. The band-structure calculations were based on the experimental crystal geometry[17−19] with and without further geometry optimizations (the cell constants were fixed at the experimental values during optimization). The density of states (DOS) was computed using the tetrahedron method with Blöch corrections and a $4 \times 16 \times 8$ and $4 \times 12 \times 6$ k-point mesh for **PFT** and **PFP**, respectively, in the Monkhorst−Pack scheme.[42] The inverse effective mass tensor was calculated using Sperling's centered difference method at the band edges with $dk = 0.16$ Å^{-1}. To corroborate the main features of the band structure described using DFT-PBE (PAW), the band structures of **PFT** and **PFP** were also computed using the B3LYP functional and the 6-21G basis set implemented in the CRYSTAL06 program.[43]

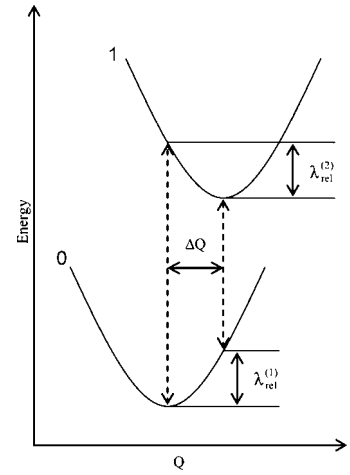

Figure 2. Sketch of the potential-energy surfaces for the neutral state 0 and the charged state 1, showing the vertical transitions (dashed lines), the normal mode displacement ΔQ, and the relaxation energies, $\lambda_{rel}^{(1)}$ and $\lambda_{rel}^{(2)}$.

3. Results and Discussion

3.1. Molecular Properties. Geometry. The molecular geometries for the neutral state of **PFT** and **PFP** were optimized under D_{2h} symmetry.[17,19] Figure S1 in the Supporting Information displays the experimental and computed bond lengths for the two perfluoroacenes. The computed bond lengths agree well with the X-ray diffraction values (i.e.,within 0.010 Å). As observed for the unsubstituted oligoacenes,[44] the degree of C−C bond-length alternation along the perimeters of the molecules increases in going from the center to the ends, while the C−C bonds parallel to the short molecular axis are rather long (except for the molecular ends). The trends obtained for **PFT** and **PFP** have also been observed in other functionalized oligoacenes.[45,46]

We now turn to a discussion of the geometry relaxations upon oxidation or reduction of **PFT** and **TET** (see Figure 3). The

(28) Reimers, J. R. *J. Chem. Phys.* **2001**, *115*, 9103.
(29) Malagoli, M.; Coropceanu, V.; da Silva, D. A.; Brédas, J. L. *J. Chem. Phys.* **2004**, *120*, 7490.
(30) Wong, M. W. *Chem. Phys. Lett.* **1996**, *256*, 391.
(31) Senthilkumar, K.; Grozema, F. C.; Bickelhaupt, F. M.; Siebbeles, L. D. A. *J. Chem. Phys.* **2003**, *119*, 9809.
(32) Valeev, E. F.; Coropceanu, V.; da Silva, D. A.; Salman, S.; Brédas, J. L. *J. Am. Chem. Soc.* **2006**, *128*, 9882.
(33) *ADF, 2006.01*; Scientific Computing and Modelling NV: Amsterdam, 2006.
(34) Bunte, S. W.; Sun, H. *J. Phys. Chem. B* **2000**, *104*, 2477.
(35) Martinelli, N. G.; Olivier, Y.; Ruiz Delgado, M. C.; Pigg, K. R.; da Silva Filho, D. A.; Sánchez-Carrera, R. S.; Venuti, E.; Della Valle, R. G.; Brédas, J. L.; Beljonne, D.; Cornil, J., in preparation.
(36) Kresse, G.; Furthmuller, J. *Comput. Mater. Sci.* **1996**, *6*, 15.
(37) Kresse, G.; Hafner, J. *Phys. Rev. B* **1993**, *47*, 558.
(38) Kresse, G.; Hafner, J. *Phys. Rev. B* **1994**, *49*, 14251.
(39) Perdew, J. P.; Burke, K.; Ernzerhof, M. *Phys. Rev. Lett.* **1996**, *77*, 3865.
(40) Blochl, P. E. *Phys. Rev. B* **1994**, *50*, 17953.
(41) Kresse, G.; Joubert, D. *Phys. Rev. B* **1999**, *59*, 1758.
(42) Monkhorst, H. J.; Pack, J. D. *Phys. Rev. B* **1976**, *13*, 5188.
(43) Dovesi, R.; Saunders, V. R.; Roetti, C.; Orlando, R.; Zicovich-Wilson, C. M.; Pascale, F.; Civalleri, B.; Doll, K.; Harrison, N. M.; Bush, I. J.; D'Arco, P.; Llunell, M. *CRYSTAL06 User's Manual*; University of Torino: Torino, 2006.
(44) Yamakita, Y.; Kimura, J.; Ohno, K. *J. Chem. Phys.* **2007**, 126.
(45) Houk, K. N.; Lee, P. S.; Nendel, M. *J. Org. Chem.* **2001**, *66*, 5517.
(46) Winkler, M.; Houk, K. N. *J. Am. Chem. Soc.* **2007**, *129*, 1805.

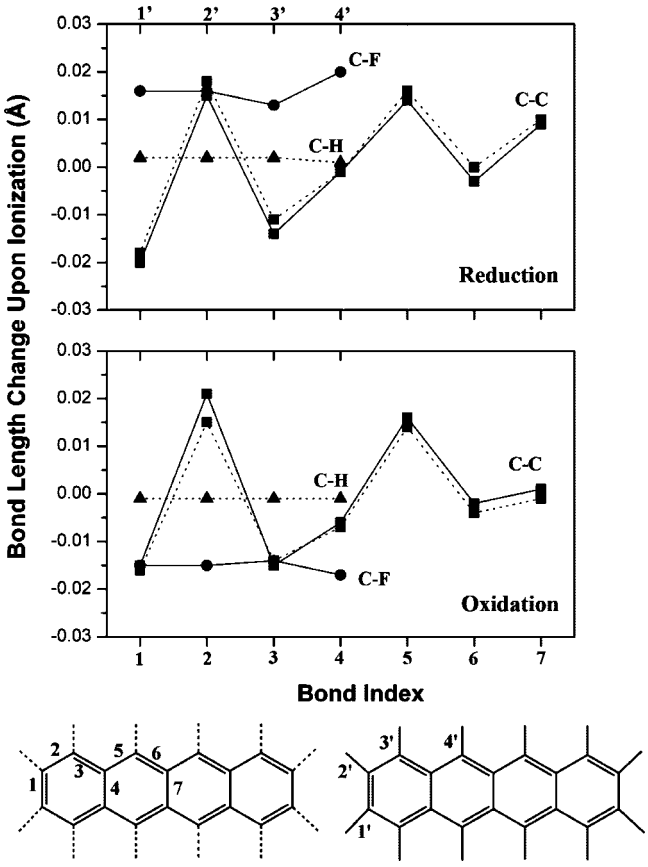

Figure 3. Calculated bond-length modifications in isolated **PFT** (solid lines) and **TET** (dashed lines) upon oxidation and reduction.

C−C bonds undergo similar geometric changes in the cationic and anionic states in both compounds;[47,48] the bond relaxations occur over the entire molecule but are more pronounced along the molecular periphery. In contrast to their unsubstituted counterparts where very small geometric changes occur for the C−H bonds, the C−F bonds undergo significant bond relaxation upon reduction or oxidation. Therefore, the major geometrical changes due to oxidation and reduction in the perfluoroacenes, **PFT** and **PFP**, involve not only the carbon atoms but also the fluorines.

Electronic Structure. The gas-phase UPS spectra of **PFT** and **PFP** are given in Figure 4. For the sake of comparison, the spectra previously reported for **TET** and **PEN** are included as well.[49] As found in unsubstituted oligoacenes, the first ionization peak shows a vibrational fine structure upon perfluorination. As expected, the first ionization energies of 7.80 and 7.50 eV for **PFT** and **PFP**, respectively, are larger (by about 0.90 eV) than those of the fluorine-free molecules, 6.94 and 6.59 eV for **TET** and **PEN**.[49]

As seen from Table 1, the evolution of the first ionization potential (IP) upon perfluorination and as a function of oligomer length is well reproduced by the calculations at both Koopmans' theorem[50] (KT) and self-consistent field (ΔSCF) levels. DFT-B3LYP calculations predict a decrease in the IP value by about 0.3 eV when going from **PFT** to **PFP**, while an increase of about 0.9 eV is calculated upon perfluorination; these results reproduce very well the experimental trends. The best agreement with experiment is achieved at the ΔSCF level using an augmented basis set with diffuse functions; in that case, the calculated IP values are systematically some 0.3 eV lower than the UPS data (i.e., the DFT-calculated vertical IP of **PFT** [**PFP**] is estimated to be 7.60 [7.21] eV, whereas the experimental first ionization peak is observed at 7.80 [7.50] eV). In addition to strongly enhanced IP, the insertion of fluorine atoms in oligoacenes also makes the electron affinities (EAs) more exothermic (i.e., according to the DFT calculations, approximately 1.20 eV more exothermic than that of the parents **TET** and **PEN**). This is consistent with the overall stabilization of both the doubly occupied and the empty frontier molecular orbitals upon perfluorination.[51] As shown in Figure 5, the majority of the molecular orbital density in the HOMO and LUMO orbitals is delocalized along the C−C backbone, but significant contributions from the fluorine atoms are also found; this is in line with the significant C−F bond relaxations observed upon oxidation or reduction (see Figure 3). These results are in excellent agreement with the electrochemical measurements; the reduction and oxidation peaks of **PFP** [**PFT**] shift positively as compared to those of **PEN** [**TET**] (by +0.74 [+0.64] and +0.57 [+0.56] eV, respectively, in 1,2-dichlorobenzene).[17,19] As the size of the system increases, the compound becomes more easily reduced (the EA of **PFP** is approximately 0.4 eV more exothermic than that of **PFT**); this is consistent with the positive shift of the reduction potential from −1.49 eV in **PFT** to −1.13 eV in **PFP**.[17,19] Thus, as one would expect, the electronegative fluorine atoms increase the stability of the substituted oligoacene anions toward reaction with water and oxygen. These results also mean that the fluorine atoms can lower the injection barriers of electrons from low workfunction metallic electrodes.

3.2. Crystal Properties. Table 2 lists the crystallographic parameters of all of the studied systems. **PEN** and **TET** crystallize in the triclinic space group *P*-1, with two molecules per unit cell.[52] In contrast, the perfluorinated counterparts are characterized by the monoclinic space group *P*21/*c*, with four and two molecules per unit cell for **PFT** and **PFP**, respectively.[17,19] Note that the axis labeling is different in the two types of crystals.

We now examine in more detail the differences in crystal packing upon perfluorination. While earlier work indicated that organic fluorine does not provide stable intermolecular interactions,[53,54] more recent investigations provide evidence for the propensity of interactions such as C−F···F′−C′, C−F···π, and C−H···F.[55−57] However, there is still no clear understanding

(47) Chen, H. Y.; Chao, I. *Chem. Phys. Lett.* **2005**, *401*, 539.
(48) Kato, T.; Yamabe, T. *J. Chem. Phys.* **2003**, *119*, 11318.
(49) Coropceanu, V.; Malagoli, M.; da Silva, D. A.; Gruhn, N. E.; Bill, T. G.; Brédas, J. L. *Phys. Rev. Lett.* **2002**, 89.
(50) Koopmans, T. *Physica* **1934**, *1*, 104.
(51) Perfluorination is observed to downshift the LUMO more than the HOMO (by 0.97 [0.96] and 0.76 [0.78] eV, respectively, in **PFT** [**PFP**]), thus leading to a narrowing of the HOMO−LUMO gap by ~0.2 eV (from 2.78 [2.21] eV in **TET** [**PEN**] to 2.57 [2.03] eV in **PFT** [**PFP**]). The overall impact of fluorine substitution on the energy levels of the frontier MOs can be rationalized on the basis of the interplay between the electron-withdrawing inductive effects and the electron-donating mesomeric effects; the former stabilize the HOMO and LUMO in a similar way, whereas the latter lead to a stronger destabilization of the HOMO with respect to the LUMO due to the low-energetic position of the p_z orbitals of fluorine. For a detailed discussion, see:Medina, B. M.; Beljonne, D.; Egelhaaf, H. J.; Gierschner, J. *J. Chem. Phys.* **2007**, *126*, 111101.
(52) Holmes, D.; Kumaraswamy, S.; Matzger, A. J.; Vollhardt, K. P. C. *Chem.-Eur. J.* **1999**, *5*, c3399.
(53) Desiraju, G. R.; Parthasarathy, R. *J. Am. Chem. Soc.* **1989**, *111*, 8725.
(54) Taylor, R.; Kennard, O. *J. Am. Chem. Soc.* **1982**, *104*, 5063.
(55) Choudhury, A. R.; Row, T. N. G. *CrystEngComm* **2006**, *8*, 265.

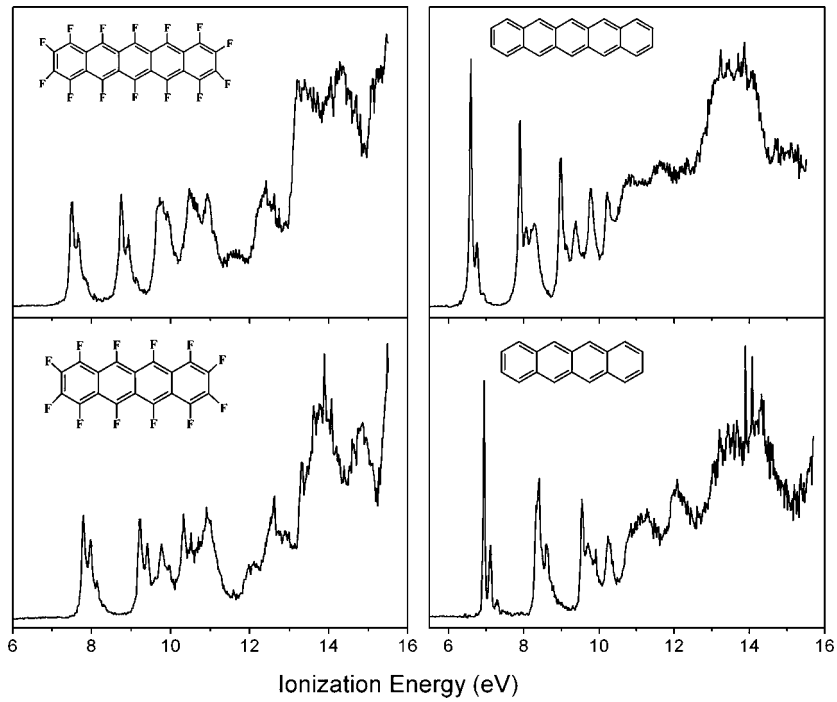

Figure 4. Gas-phase UPS spectra of **PFP** and **PFT** (this work) and of **PEN** and **TET** (from ref 49).

Table 1. First Ionization Potentials (IPs) and Electron Affinities (EAs) for Isolated **PFT**, **PFP**, **TET**, and **PEN** Molecules Obtained from ΔSCF and KT Calculations at the B3LYP/6-31G** Level[a]

	IP [eV]				EA[b] [eV]		
	vertical	adiabatic	Koopmans	exp.[c]	vertical	adiabatic	Koopmans
PFT	7.08 (7.60)	6.95 (7.47)	5.63 (6.17)	7.80[d]	−1.58 (−2.20)	−1.72 (−2.38)	−3.06 (−3.62)
TET	6.34 (6.56)	6.28 (6.51)	4.87 (5.14)	6.94[e]	−0.63 (−1.01)	−0.71 (−1.09)	−2.09 (−2.39)
PFP	6.71 (7.21)	6.60 (7.12)	5.39 (5.92)	7.50[d]	−2.02 (−2.63)	−2.14 (−2.78)	−3.36 (−3.93)
PEN	5.95 (6.17)	5.90 (6.13)	4.61 (4.88)	6.59[e]	−1.07 (−1.42)	−1.14 (−1.49)	−2.40 (−2.69)

[a] B3LYP/6-31++G**//B3LYP/6-31G** values are given in parentheses. [b] We have used the definition of EA as the energy change for the process $M + e^- \rightarrow M^{\bullet -}$; hence, the negative values indicate exothermicity for the reduction of a molecule. [c] Estimated from gas-phase UPS spectra. [d] This work. [e] From ref 49.

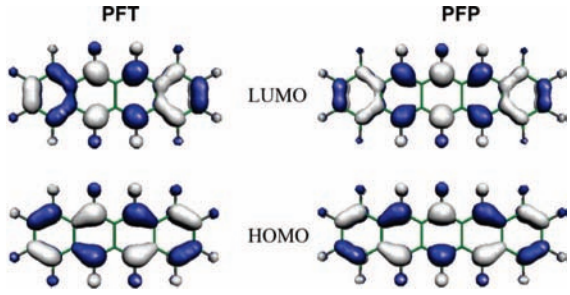

Figure 5. B3LYP/6-31G** wave functions of the frontier molecular orbitals in isolated **PFT** and **PFP**.

of the impact of fluorination on the oligoacene crystal structure and, thus, on charge transport. The electrostatic surface potentials (see Figure 6) indicate that, while the unsubstituted acenes display a typical π-cloud, the perfluorinated compounds feature an inverse electron density distribution (the centers of the acene rings are now electron-deficient, while the locations of the fluorine atoms are electron-rich). Such a pronounced difference in the electrostatic surface potentials can trigger a modification

Table 2. Crystallographic Parameters for the Unit Cells of **TET**,[52] **PEN**,[52] **PFT**,[19] and **PFP**[17]

	a[a]	*b*	*c*	α[b]	*β*	*γ*
TET	6.06	7.84	13.01	77.13	72.12	85.79
PEN	6.28	7.71	14.44	76.75	88.01	84.52
PFT	26.75	4.59	11.48	90	101.43	90
PFP	15.51	4.49	11.45	90	91.57	90

[a] Units in angstroms. [b] Units in degrees.

of the crystalline packing arrangements. As illustrated in Figure 7, both perfluorinated and unsubstituted acenes present a herringbone motif in the *bc* (or *ab*) planes; however, there are significant differences that are prompted by the introduction of the fluorines atoms:

(i) The molecular planes of adjacent molecules along the herringbone diagonal axis form an angle of ∼52° [51°] in **PEN** [**TET**], while these molecules are nearly perpendicular (∼91°) in the perfluorinated crystals. The configuration observed in the perfluoroacenes is consistent with C−F···F′−C′ interactions between the edge-to-face rings[58] [the F···F distances (3.00 Å) are on the order of the sum of the van der Waals radii (2.94 Å)].

(ii) Although the interplanar distance within the π-stacks in **PFT** and **PFP** (∼3.25 Å) is larger than that found in **PEN** (∼2.55 Å), the displacements along the short molecular axis are much less pronounced, and no long-axis sliding is observed

(56) Prasanna, M. D.; Row, T. N. G. *Cryst. Eng.* **2000**, *3*, 135.
(57) Reichenbacher, K.; Suss, H. I.; Hulliger, J. *Chem. Soc. Rev.* **2005**, *34*, 22.

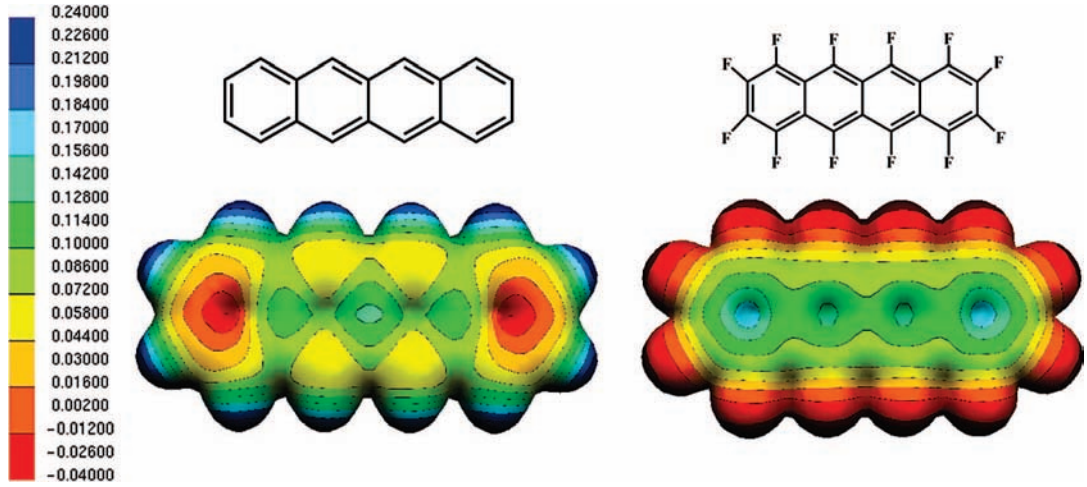

Figure 6. B3LYP/6-1G** electrostatic surface potentials mapped onto a surface of total electron density for **TET** (left) and **PFT** (right). Regions of higher electron density are shown in red and of lower electron density in blue (values in atomic units).

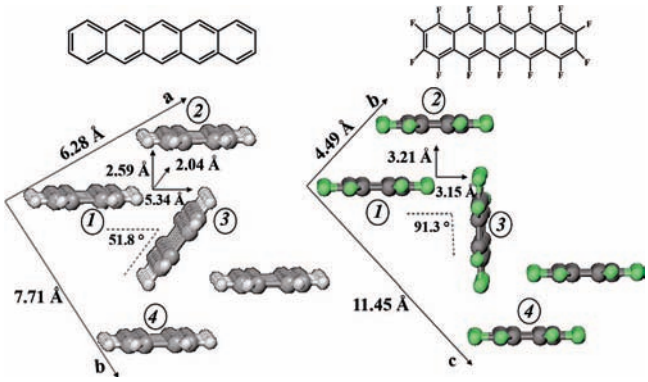

Figure 7. Illustration of the lattice parameters within the *ab* [*bc*] layer of crystalline **PEN** [**PFP**] based on the X-ray structures of refs 52 and 17. The short-axis and long-axis displacements along the π-stacks in the *a* [*b*] direction are also indicated. The labeling of the molecules used in the calculations of the transfer integrals is also shown.

upon perfluorination (see Figure 7). Such a better cofacial stacking, likely supported by interactions between electronegative fluorine atoms and the electropositive center of a perfluorinated ring, in turn impacts the electronic couplings, as we discuss below.

Transfer Integrals. Whether transport occurs through a band-like or hopping mechanism, the electronic coupling plays a major role in the determination of the charge carrier mobility. Here, we have applied a methodology discussed in detail earlier[32] to evaluate the effective transfer integrals (electronic coupling matrix elements), *t*.

The transfer integrals calculated for nearest-neighbor pairs of molecules along various crystal directions are collected in Table 3. It is useful to note that the transfer integral values reported here for isolated dimers practically coincide with those for dimers embedded in extended clusters; see the Supporting Information. In agreement with reported values,[59,60] the largest electronic couplings for **PEN** and **TET** are derived for dimers along the diagonal directions within the *ab*-plane (dimers 1,3 and 2,3 in Figure 7); the *t* values, however, remain significant between cofacial dimers along the *a*-direction. Interestingly, this picture radically changes upon perfluorination; the largest transfer integrals are obtained between neighboring π-stack molecules along the *b*-direction (−132 and 73 meV for holes and electrons, respectively, for a **PFP** dimer), while very small electronic couplings are found between face-to-edge dimers within the *bc*-plane. For comparison, the electronic coupling between π-stacked dimers (molecules 1 and 2 in Figure 7) increases by a factor of ∼4 [2] for holes [electrons] in **PFP** versus that of the parent **PEN**, whereas values up to 40 times smaller are found for the face-to-edge dimers along the diagonal directions (dimers 1,3 and 2,3). This result is not surprising because the electronic coupling is driven by wave function overlap, which is expected to be much higher in a 51°-tilted **PEN** dimer than in the perpendicular (∼91°) **PFP** dimer. The transfer integrals are larger in the crystal of the more extended oligomer **PFP**, which is consistent with the better device performance exhibited in OTFTs based on **PFP** than on **PFT** (electron mobilities of ca. 0.22 vs 0.00024 $cm^2/(V \cdot s)$).[17,19]

To better understand the differences in the electronic couplings of the unsubstituted and perfluorinated oligoacenes, we have analyzed the impact of translations along the short molecular axis. Figure S3 in the Supporting Information shows the evolution of the HOMO and LUMO transfer integrals calculated for cofacial dimers of **PFT** and **PFP** when the top molecule is translated along its short molecular axis at an intermolecular distance fixed to the value observed in the crystal structure along the *b*-direction. It is important to note that small displacements can lead not only to a significant change in the amplitude of the transfer integral but also to a change in its sign, which is specifically the case here for the HOMO. These evolutions can be rationalized by examining the wave functions of the frontier molecular orbitals (see Figure 5). The HOMO wave functions change sign along the short axis, which leads to the appearance of two minima in the course of the translation. In contrast, the LUMO wave functions over the conjugated C−C backbone do not change sign along the short axis. As a result, the LUMO transfer integral decreases gradually as the translation proceeds, until it reaches zero for a shift of 4 Å where perfect cancellation between bonding and antibonding orbital overlap occurs; the couplings then slightly increase again in the range of 4−5.5 Å where antibonding C−F interactions become

(58) Ramasubbu, N.; Parthasarathy, R.; Murrayrust, P. *J. Am. Chem. Soc.* **1986**, *108*, 4308.
(59) Cornil, J.; Beljonne, D.; Calbert, J. P.; Brédas, J. L. *Adv. Mater.* **2001**, *13*, 1053.
(60) Coropceanu, V.; Cornil, J.; da Silva, D. A.; Olivier, Y.; Silbey, R.; Brédas, J. L. *Chem. Rev.* **2007**, *107*, 2165.

Table 3. DFT-PW91-Calculated Transfer Integrals (in meV) for HOMO (t_H) and LUMO (t_L) in **PFT** and **PFP** (Left), and **TET** and **PEN** (Right)[a]

	PFT		PFP			TET		PEN	
dimers	t_H	t_L	t_H	t_L	dimers	t_H	t_L	t_H	t_L
1,2 (*b*-axis)	−102	61	−132	73	1,2 (*a*-axis)[d]	36/16	−13/−32	34/37	−42/−45
1,4 (*c*-axis)	0	0	0	0	1,4 (*b*-axis)	0	0	0	−1
1,3 (*bc*-plane)[b]	−2	2	−2	−3	1,3 (*ab*-plane)[b]	−23	65	−51	−82
2,3 (*bc*-plane)[b]	−2	2	−2	−3	2,3 (*ab*-plane)[b]	70	64	85	81
a-axis[c]	0	−3	3	−7	*c*-axis[e]	0	0	0	0

[a] The crystal direction along which the coupling takes place is also indicated in parentheses. [b] The coupling here corresponds to the diagonal directions of the *bc*- or *ab*-plane. [c] Nearest-neighbor pair along the *a*-direction. [d] Because of the presence of two geometrically inequivalent molecules in the unit cell of **TET** and **PEN**, two different electronic coupling values are obtained along the *a*-axis. [e] Nearest-neighbor pair along the *c*-direction.

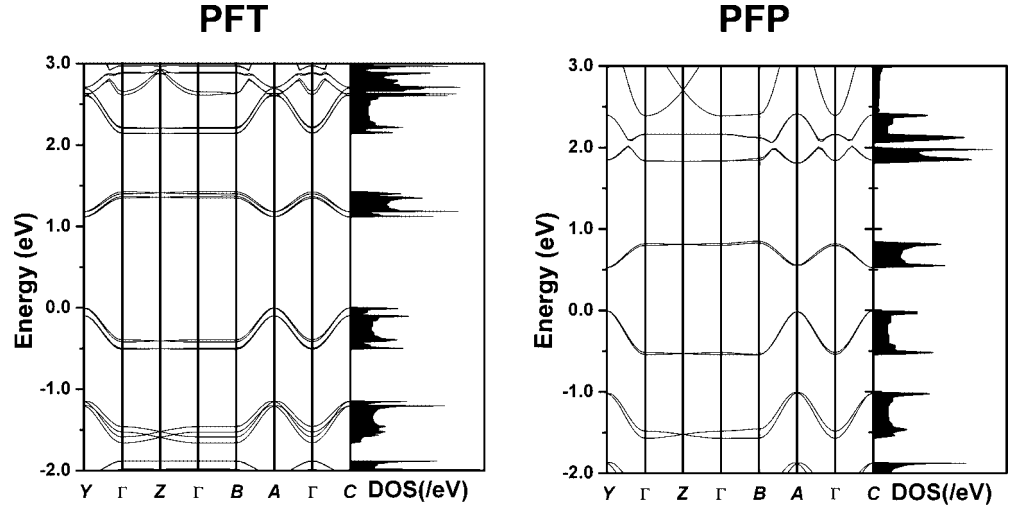

Figure 8. DFT/GGA-PW91-PAW band structure and density of states of **PFT** (left) and **PFP** (right). Points of high symmetry in the first Brillouin zone are labeled as follows: Γ = (0,0,0), *A* = (0.5,0.5,0), *B* = (0.5,0,0), *C* = (0,0.5,0.5), *Y* = (0,0.5,0), and *Z* = (0,0,0.5), all in crystallographic coordinates.

dominant. An important consequence of this difference in oscillation period is that the displacement of 3.2/3.25 Å observed in the **PFP/PFT** crystal lies rather close to a maximum in the electronic coupling for the HOMO, while the LUMO transfer integral values are ∼70 meV; this leads to a situation where both electrons and holes can be expected to be mobile. These results clarify the origin of the significant transfer integrals calculated along the *b*-direction in **PFT** and **PFP** crystals (see Table 3). In unsubstituted acene crystals, by contrast, the short-axis displacements are so large (i.e., 5.34 [5.31] Å in **PEN** [**TET**]; see Figure 7) that adjacent π-stacked molecules along the *a*-direction interact weakly, and the calculated HOMO and LUMO electronic couplings between face-to-face dimers are significantly smaller than those of the perfluorinated compounds (for instance, t_H = 34/37 meV for dimers 1,2 in **PEN** versus −132 meV for **PFP**; see Table 3).

Band Structure. The electronic band structures of the **PFP** and **PFT** crystals are shown in Figure 8 along the reciprocal lattice vectors and several specific directions on the surface of the first Brillouin zone. The upper HOMO band is separated from the lower LUMO band by a direct bandgap at the C point. As expected and in agreement with experimental data, a decrease in bandgap is observed with increasing the acene length; the HOMO−LUMO gaps obtained from the redox potentials decrease by 0.59 eV when going from **PFT** to **PFP**,[17,19] which corresponds exactly to the calculated difference in bandgap, 1.1 eV in **PFT** versus 0.52 eV in **PFP**. While, as is well-known, the GGA-PW91-PAW method underestimates the band gap in comparison to experiment (the HOMO−LUMO gap obtained from the redox peaks is 1.92 [2.51] eV for **PFP** [**PFT**]),[17,19] we underline that the main characteristics of the valence and conduction bands are not affected.[61]

The conduction and valence bands of **PFP** consist of two nearly degenerate π-sub-bands that arise from the presence of the two inequivalent **PFP** molecules in the unit cell. **PFT** has four molecules per unit cell, and two are geometrically inequivalent; as a result, both valence and conduction bands split into sub-bands quasi-degenerate two by two (note that a constant sub-band splitting of 80 and 30 meV is found for the valence and conduction bands, respectively). However, in both crystals, the shapes of the conduction and valence bands are very similar, and a strong orientational anisotropy of the band dispersion is observed. The largest valence/conduction band dispersions occur along the *b*-axis (in the Γ*Y* section of the Brillouin zone), while a flat band is observed along the *c*-axis (Γ*Z*) and along the direction perpendicular to the molecular layer (Γ*B*). These results are consistent with the transfer integral calculations (see Table 3), where significant electronic couplings are found only for the π-stacked dimers along the *b*-axis (dimers 1,2). The large band dispersions in *A*Γ (*ab*-plane) and Γ*C* (*bc*-plane) can also be explained by π−π coupling between molecules 1 and 2 (see Figure 7). As a result of the strong anisotropy in the intermolecular interactions, the full valence [conduction] bandwidth

(61) The band structure and DOS spectrum of **PFP** and **PFT** were computed as well using the hybrid B3LYP functional with a 6-21 G atomic orbital basis set implemented in the CRYSTAL06 program. The main feature of the valence and conduction electronic structure was fully consistent with those calculated using the VASP program (with a B3LYP direct gap of 1.32/2.07 eV and slightly larger valence and conduction bandwidths, which amount to 0.635/0.571 and 0.486/0.429 eV for **PFP** and **PFT**, respectively).

Table 4. Hole and Electron Effective Masses m (in Units of the Electron Mass at Rest, m_0) at the Band Extrema of the **PFT** and **PFP** Crystals

	m/m_0	parallel to
PFT[a]		
holes at C		$a + 0.064c$
	1.69	b
	70.69	$c - 0.560a$
electrons at C		$a + 0.069c$
	2.88	b
	48.44	$c - 0.590a$
PFP		
holes at C	11.06	$a + 0.017c$
	1.22	b
	55.30	$c - 0.006a$
electrons at C	4.22	$a + 0.029c$
	2.08	b
	67.14	$c - 0.001a$

[a] Because of the flatness of the band, we were unable to derive an accurate value of the effective mass along the a-crystallographic direction for the **PFT** crystal.

(0.53 [0.28] eV for **PFP**) is in excellent agreement with the value derived from a one-dimensional tight-binding model along the b-axis ($4t_H = 0.53$ eV and $4t_L = 0.29$ eV for **PFP**).

Importantly, when comparing the band structures of **PFP** and **PEN**,[62,63] significant differences are found. In contrast to the quasi-degeneracy of the valence (conduction) band found in the **PFP** crystal, a significant valence [conduction] sub-band splitting is observed in the **PEN** crystal; this splitting is related to the significant electronic coupling between translationally inequivalent molecules along the diagonal directions within the herringbone plane (see Figure 7 and Table 3). This result is consistent with the large band dispersions observed in **PEN** not only along the a-axis, as expected from the π-stacking in this direction, but also along the b-axis and within the herringbone ab-plane; thus, charge transport has more of a two-dimensional character in **PEN** crystals.

Effective Mass. We apply here the concept of effective mass to describe the charge-transport characteristics in the perfluorinated crystals. In the case of wide bands where excess electrons [holes] occupy states near the bottom [top] of the conduction [valence] band, the mobility is governed by the effective masses that can be computed from the band structures at the band extrema (thermally populated levels). The inverse effective mass tensor m_{ji}^{-1} is given by:[64]

$$\frac{1}{m_{ij}} = \frac{1}{\hbar^2}\frac{\partial^2 E}{\partial k_j \partial k_i} \tag{6}$$

where subscripts i and j denote the Cartesian coordinates in reciprocal space, E the band energy, $\hbar$ the Planck constant, and k the electron wavevector.

The hole and electron effective masses for the **PFP** and **PFT** crystals are reported in Table 4. The smallest effective masses for both holes and electrons are found along the b-axis, in agreement with the transfer integral calculations. The effective masses along the other directions, except for electrons along the a-axis in the **PFP** crystal, are much larger than those along the b-axis. Effective masses for both electrons and holes in **PFP** are found to be smaller than those in **PFT**, which correlates with experimental data.[19] It is interesting to note that the estimated effective mass of $1.22m_o$ for holes in **PFP** is even smaller than that found in **PEN**.[62]

Table 5. Reorganization Energies λ (in eV), Associated with Hole- and Electron-Vibrational Couplings, Calculated at the B3LYP/6-31G** Level

	λ (holes)		λ (electrons)	
	AP[a]	NM[b]	AP	NM
PFT	0.258	0.259	0.289	0.286
PFP	0.222	0.222	0.224	0.225

[a] Values calculated from the adiabatic potential (AP) surfaces for the neutral and charged species. [b] Values obtained from a normal-mode (NM) analysis.

3.3. Vibronic Coupling. The vibronic (electron−phonon) interaction is another key factor that has a strong effect on the charge transport. In organic semiconductors, there are two major electron−phonon mechanisms: the first arises from the modulation of the site energies by vibrations and is referred to as local coupling, while the second mechanism arises from the modulation of the transfer integrals by intermolecular vibrations and is referred to as nonlocal coupling.[65,66]

We first focus on the local electron−phonon mechanism. The overall strength of this coupling is expressed by the polaron binding (relaxation) energy E_{pol} or, in the context of electron transfer theory, by the reorganization energy λ ($\sim 2E_{pol}$). It consists of both intra- and intermolecular contributions; the former reflect the changes in the geometry of individual molecules and the latter in the polarization of the surrounding molecules, upon going from the neutral to the charged state and vice versa. In the case of nonpolar organic systems, the impact of the surrounding comes from the modulation of the electronic polarization energy by intermolecular vibrations. Previous results reported by Brovchenko[67] as well as our recent work on the naphthalene crystal using a QM/MM approach[68] underline that the intermolecular contributions are expected to be much smaller than those of the intramolecular contributions. This is the reason why we consider here only the intramolecular contributions to the local coupling.

Table 5 collects the DFT estimates of the reorganization energies associated with hole- and electron-vibrational couplings calculated from the adiabatic potentials (AP) and from the normal-mode analysis (NM); the results of the two approaches are in excellent agreement. The comparison of the data for **PFT** and **PFP** with those obtained previously for tetracene and pentacene[29,49] shows that upon perfluorination λ increases by about a factor of 2 for both holes and electrons. It is important to underline that the calculated electron reorganization energy of **PFP** (0.222 eV), which agrees with previous calculations,[47] remains smaller than the values calculated for many other organic systems considered as good electron-transport materials. For instance, values of 0.272 eV were reported for PTCDI-C5 {*N*,*N*′-dipentyl-3,4,9,10-perylene tetracarboxylic diimide},[69] and 0.49−0.56 eV for 1,1-diaryl-2,3,4,5-tetraphenylsiloles.[70]

As in our previous work,[29,49] the couplings were analyzed via a decomposition of the reorganization energies into contri-

(62) de Wijs, G. A.; Mattheus, C. C.; de Groot, R. A.; Palstra, T. T. M. *Synth. Met.* **2003**, *139*, 109.
(63) Hummer, K.; Ambrosch-Draxl, C. *Phys. Rev. B* **2005**, *72*, 205205.
(64) Seeger, K. *Semiconductor Physics: An Introduction*, 9th ed.; Springer-Verlag: Berlin, 2004.
(65) Pope, M.; Swenberg, C. E. *Electronic Processes in Organic Crystals and Polymers*, 2nd ed.; Oxford University Press: New York, 1999.
(66) Silinsh, E. A.; Čápek, V. *Organic Molecular Crystals: Interaction, Localization, and Transport Phenomena*, 2nd ed.; AIP Press: New York, 1994.
(67) Brovchenko, I. V. *Chem. Phys. Lett.* **1997**, *278*, 355.
(68) Norton, J. E.; Brédas, J. L. *J. Am. Chem. Soc.* **2008**, *130*, 12377.

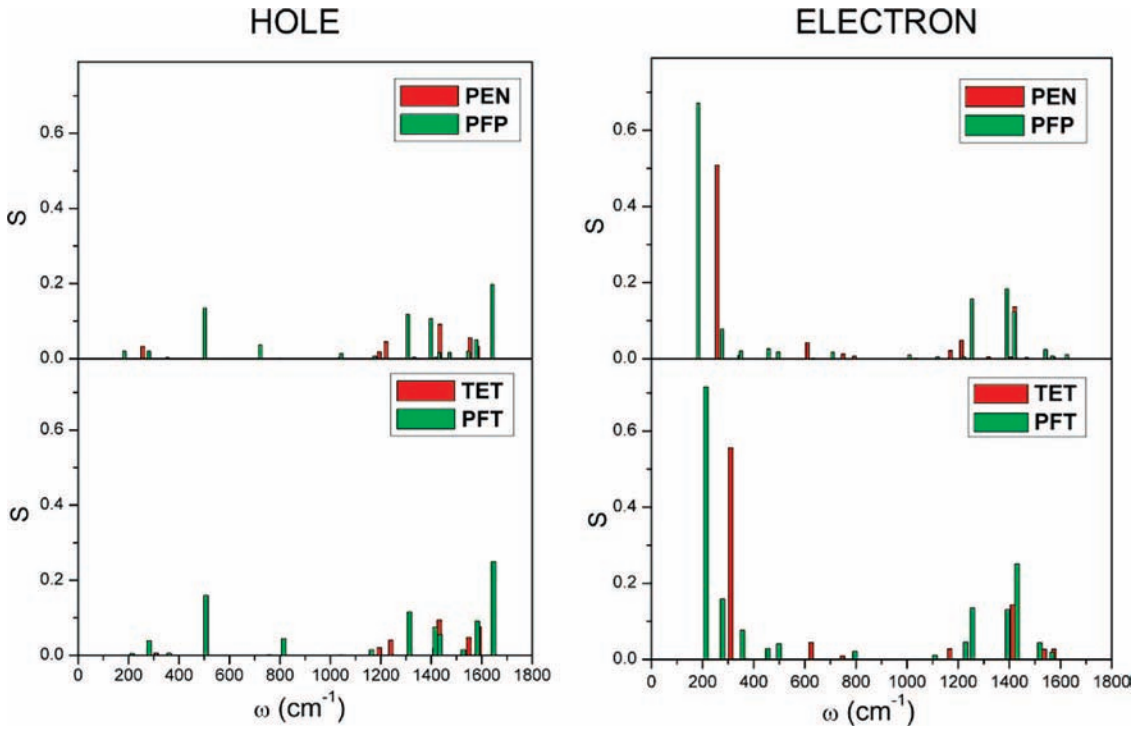

Figure 9. DFT-B3LYP/6-31G** Huang−Rhys factors (S_i) related to hole and electron transfers, as a function of normal-mode frequency.

Table 6. Values of *L* (in meV), Average of the Transfer Integrals, and Standard Deviation for Representative Dimers (Dimers 1,2 and 2,3 in Figure 7) in the **PFT** and **PFP** Crystals

	PFT			PFP			PFT			PFP		
dimers	σ_H	$\langle t_H \rangle$	L_H	σ_H	$\langle t_H \rangle$	L_H	σ_L	$\langle t_L \rangle$	L_L	σ_L	$\langle t_L \rangle$	L_L
cofacial (*b*-axis)	44	−134	39	43	−135	37	31	98	19	33	107	22
face-to-edge (*bc*-plane)	5	3	<1	5	3	<1	3	<1	<1	3	−1	<1

butions of each normal mode. The vibrational couplings (Huang−Rhys factors, S_j) related to the hole and electron transfer in **PFP**, **PFT**, **PEN**, and **TET** are illustrated in Figure 9 (see also the Supporting Information for the numerical values). The results for the electron-vibration coupling constants are in agreement with previous theoretical studies by Kato and Yamabe,[48,71] who used an alternate approach based on the concept of orbital vibronic coupling constant.[72]

As found in unsubstituted oligoacenes,[29,73] the reorganization energy related to hole transfer is dominated by high-energy normal modes; however, the modes below 1200 cm^{-1} start to play a larger role in fluorinated acenes, accounting for 15% of λ in **PFP** versus 2% in **PEN**. The C−C/C−F stretching modes at 1639 cm^{-1} in **PFT** and 1636 cm^{-1} in **PFP** (see the vibrational eigenvectors in Figure S4 in the Supporting Information) provide the largest contributions (39% and 35%, respectively) to the total relaxation energy. These calculations indicate that the hole reorganization energy is expected to increase through F substitution, due to C−C/C−F stretching modes around 1600 cm^{-1}, which also yield the largest Huang−Rhys factor.

In the case of electrons, as observed as well for unsubstituted oligoacenes,[29,73] the largest electron-vibrational constants (Huang−Rhys factors) are due to the coupling with the lowest-energy totally symmetric mode (at 205 cm^{-1} in **PFT** and 177 cm^{-1} in **PFP**). However, the dominant contribution to the reorganization energy is coming as in the case of holes from high-frequency vibrations above 1200 cm^{-1} (76% in **PFT** and 79% in **PFP**); the most strongly coupled high-frequency vibrations for **PFP** are shown in Figure S4.

Thus, for the perfluorinated acenes, we find that: (i) the larger reorganization energy in comparison to the unsubstituted counterparts is due to contributions from C−C/C−F stretching modes; these modes are distributed over a large energy range (1200−1600 cm^{-1}); (ii) as the size of the system increases, that is, when going from **PFT** to **PFP**, λ decreases as expected (by ∼0.35 eV in the case of holes and ∼0.6 eV in the case of electrons); (iii) due to the good match between, on the one hand, the charge densities and orientations of the HOMO and LUMO bonding/antibonding patterns and, on the other hand, the displacements along the C−C/C−F normal modes (see Figures 5 and S4), both hole- and electron-vibration couplings become larger upon perfluorination.

The shape of the first ionization band is directly related to the geometry modifications induced upon removing one electron from the system; therefore, analysis of this band provides a good

(69) Chesterfield, R. J.; McKeen, J. C.; Newman, C. R.; Ewbank, P. C.; da Silva, D. A.; Brédas, J. L.; Miller, L. L.; Mann, K. R.; Frisbie, C. D. *J. Phys. Chem. B* **2004**, *108*, 19281.
(70) Zhan, X. W.; Risko, C.; Amy, F.; Chan, C.; Zhao, W.; Barlow, S.; Kahn, A.; Brédas, J. L.; Marder, S. R. *J. Am. Chem. Soc.* **2005**, *127*, 9021.
(71) Kato, T.; Yamabe, T. *J. Chem. Phys.* **2004**, *121*, 2356.
(72) Bersuker, I. B. *Chem. Rev.* **2001**, *101*, 1067.
(73) Kwon, O.; Coropceanu, V.; Gruhn, N. E.; Durivage, J. C.; Laquindanum, J. G.; Katz, H. E.; Cornil, J.; Brédas, J. L. *J. Chem. Phys.* **2004**, *120*, 8186.

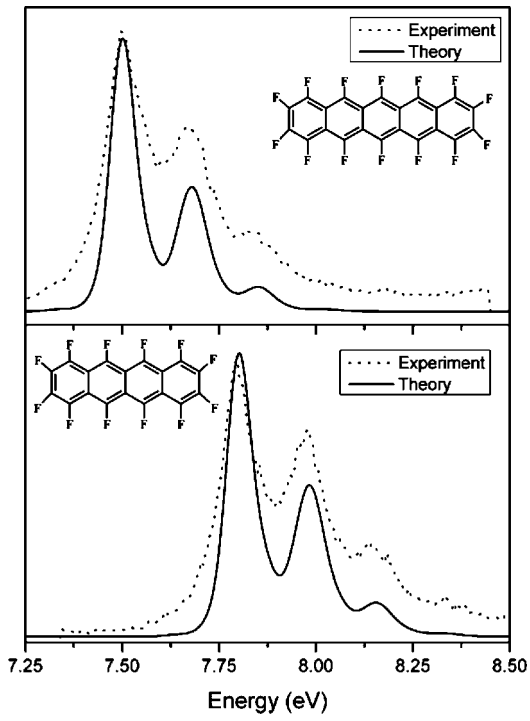

Figure 10. High-resolution close-up and DFT-B3LYP/6-31G** simulation of the vibrational structure of the first ionizations of **PFP** and **PFT**.

way to estimate the relaxation energy.[74] Upon perfluorination, the relative intensity of the vibrational peaks with respect to the 0−0 transition becomes larger (see Figure 4); this is consistent with the stronger vibrational couplings predicted by the DFT-derived Huang−Rhys factors and reorganization energies, as discussed above. This conclusion is also supported by the ability, based on DFT-calculated frequencies and Huang−Rhys factors, to simulate accurately the shape of the first ionization band of the UPS spectra in **PFT** and **PFP**. The results of the simulation performed in the framework of the Born−Oppenheimer and Franck−Condon (FC) approximations (see ref 29 for more details) are shown in Figure 10. In general, the positions and shapes of the peaks are very well reproduced. However, the intensity of the high-energy vibrational peaks is somewhat underestimated. Our previous studies at the DFT-B3LYP level on oligoacenes and thiophene-based systems[75−77] show that a better agreement with experiment is obtained when considering a 20−30% increase of the Huang−Rhys factors and resulting reorganization energies. Therefore, the reorganization energies given in Table 5 have to be considered as lower limits.

We now turn to the issue of nonlocal coupling. This mechanism is in general less well studied and understood than that of local coupling. A systematic investigation of nonlocal coupling would require the knowledge of the phonon spectra; however, a good estimate of the overall strength of the nonlocal contribution (L) can be derived by considering the variance of the transfer integrals due to thermal fluctuations, $\sigma^2 = \langle(\langle t\rangle - t)^2\rangle_{vib}$ (here, $\langle.....\rangle_{vib}$ represents the average over vibrational coordinates).[78−80] At high temperature, the following relationship holds:[78]

$$L = \frac{\sigma^2}{2k_B T} \tag{7}$$

L has a physical meaning similar to that of the reorganization energy in the case of local coupling. The average values of the related transfer integrals were estimated here using the combined quantum chemistry and molecular dynamics approach proposed by Troisi and Orlandi.[81] The standard deviation of the transfer integrals σ, the average value $\langle t\rangle_{vib}$, and L are reported in Table 6 for two representative dimers in the **PFT** and **PFP** crystals at room temperature. The largest values of L for electrons and holes (in both **PFT** and **PFP** crystals) are obtained along the b-axis; the values for holes are nearly 2 times as large as for electrons. In the case of **PEN**, the largest L values are obtained for herringbone dimers: 21 and 11 meV for holes and electrons, respectively. As in the case of the local coupling, the strength of nonlocal coupling increases by a factor of about 2 upon perfluorination; however, the ratio of the modulation of the transfer integrals due to thermal fluctuations (σ) over the average values, $\sigma/\langle t\rangle_{vib}$, is very similar in both perfluorinated and unsubstituted oligoacenes (0.33 [0.31] for holes [electrons] in **PFT** and **PFP**, and 0.35 [0.35] in **PEN**). These results suggest that the nonlocal electron−phonon couplings should be similar in both unsubstituted and perfluorinated acenes. However, a comprehensive picture can only be obtained by using a polaron model, which includes both local and nonlocal electron−phonon coupling mechanisms.

4. Conclusion

The role of perfluorination on the charge-transport properties of oligoacene crystals has been investigated by using gas-phase UPS and DFT calculations on perfluorotetracene and perfluoropentacene.

The experimental UPS data show that the first ionization energy increases by about 0.9 eV upon perfluorination; this trend is well reproduced by the DFT calculations, which also predict more exothermic electron affinities (by ca. 1 eV), in good agreement with electrochemical measurements.[17,19] The intramolecular reorganization energies calculated from the adiabatic potential energy surfaces are found to be twice as large in the fluorinated systems, due to contributions from the C−C/C−F stretching modes in the 1200−1600 cm^{-1} range. This result is supported by the ability of Franck−Condon simulations (based on DFT-calculated frequencies and Huang−Rhys factors) to reproduce the shape of the first ionization band.

The transfer-integral and band-structure calculations indicate that the largest electronic couplings in the perfluoroacene crystals are found between molecules stacked along the b-axis in a displaced cofacial configuration; accordingly, the lowest effective masses for both holes and electrons are found along these π-stacks. The strength of the nonlocal electron−phonon couplings increases by a factor of 2 upon perfluorination. However, the ratio of the modulations of the transfer integrals by intermolecular vibrations over their average value, $\sigma/\langle t\rangle_{vib}$, is

(74) Gruhn, N. E.; da Silva, D. A.; Bill, T. G.; Malagoli, M.; Coropceanu, V.; Kahn, A.; Brédas, J. L. *J. Am. Chem. Soc.* **2002**, *124*, 7918.
(75) da Silva, D. A.; Coropceanu, V.; Fichou, D.; Gruhn, N. E.; Bill, T. G.; Gierschner, J.; Cornil, J.; Brédas, J. L. *Philos. Trans. R. Soc. London, Ser. A* **2007**, *365*, 1435.
(76) Kim, E. G.; Coropceanu, V.; Gruhn, N. E.; Sanchez-Carrera, R. S.; Snoeberger, R.; Matzger, A. J.; Brédas, J. L. *J. Am. Chem. Soc.* **2007**, *129*, 13072.
(77) Sanchez-Carrera, R. S.; Coropceanu, V.; da Silva, D. A.; Friedlein, R.; Osikowicz, W.; Murdey, R.; Suess, C.; Salaneck, W. R.; Brédas, J. L. *J. Phys. Chem. B* **2006**, *110*, 18904.
(78) Coropceanu, V.; Sanchez-Carrera, R. S.; Paramonov, P.; Day, G. M.; Brédas, J.-L., submitted.
(79) Gosar, P.; Choi, S. I. *Phys. Rev.* **1966**, *150*, 529.
(80) Troisi, A. *Adv. Mater.* **2007**, *19*, 2000.
(81) Troisi, A.; Orlandi, G. *J. Phys. Chem. A* **2006**, *110*, 4065.

found to be nearly equal in both perfluorinated and unsubstituted systems; this suggests that the impact of nonlocal electron−phonon coupling is similar in both types of compounds.

Our calculations also show that perfluorination leads to an increase by a factor of about 2 in the hole- and electron-vibration couplings, but only to a moderate increase in the electronic couplings. Thus, these results suggest that the intrinsic hole and electron mobilities might be lower in the perfluorinated acene crystals. However, a full description of the charge-transport properties and their temperature dependence would require a treatment that includes polaronic models in which both local and nonlocal electron−phonon couplings are considered.

Finally, for the perfluorinated crystals, we found larger electronic couplings for holes than for electrons but similar electron−phonon couplings. Thus, these results point to hole mobilities that could even be larger than electron mobilites. As a consequence, these materials have the potential to act as ambipolar charge transporters under the proper operating conditions.

Acknowledgment. The work at Georgia Tech has been primarily supported by the National Science Foundation through the MRSEC Program under Award Number DMR-0212302, as well as through the CRIF Program under Award CHE-0443564; the work at the University of Málaga was supported in part by the Dirección General de Enseñanza Superior (DGES, MEC, Spain) through research Project CTQ2006-14987-C02-01, and by the Junta de Andalucía for Project P06-FQM-01678. M.C.R.D. acknowledges the Spanish Ministry of Education and Science (MEC) for a MEC/Fulbright Postdoctoral Fellowship at the Georgia Institute of Technology. R.M.O. is grateful to the MEC for a FPU grant, and J.C. for an I3 Professorship of Chemistry position at the University of Málaga, respectively. We are grateful to the Minnesota Supercomputing Institute for use of their computational facilities.

Supporting Information Available: B3LYP/6-31G** and averaged X-ray bond lengths of **PFT** and **PFP** (Figure S1); transfer integral results for extended systems (Figure S2); evolution of the transfer integrals in **PFT** and **PFP** cofacial dimers as a function of the degree of translation of one molecule along its short molecular axis (Figure S3); normal modes with strong hole and electron vibrational couplings in **PFP** (Figure S4); B3LYP/6-31G** estimates of vibrational frequencies (ω) and Huang−Rhys factors (S_i) related to hole and electron transfers in **PFT** and **PFP** (Tables S1 and S2); Cartesian coordinates and energies of all calculated structures; and the complete ref 25. This material is available free of charge via the Internet at http://pubs.acs.org.

JA807528W